remote sensing

MDPI

Article

Enhancing FY-3E/VASS Humidity Profiles During a Cloudy Atmospheric River Event Using Clear-Sky FY-4B/GIIRS Guidance

Hanzhen Yan [1,2], Jieying He [1,*] and Yang Guo [3]

[1] Key Laboratory of Microwave Remote Sensing, National Space Science Center, Chinese Academy of Sciences, Beijing 100190, China; yanhanzhen25@mails.ucas.ac.cn
[2] University of Chinese Academy of Sciences, Beijing 100049, China
[3] Key Laboratory of Radiometric Calibration and Validation for Environmental Satellites, The Innovation Center for FengYun Meteorological Satellite (FYSIC), National Satellite Meteorological Center (National Center for Space Weather), China Meteorological Administration, Beijing 100081, China; guoyang@cma.gov.cn
* Correspondence: hejieying@mirslab.cn

Highlights

What are the main findings?

- A clear-sky-guided correction framework was developed to enhance FY-3E/VASS humidity profiles under cloudy conditions by combining low-dimensional residual modeling, neural-network prediction, target-day calibration, and cloud-condition adjustment.
- The enhanced FY-3E/VASS humidity profiles show improved agreement with the ERA5 reference in both the cloudy high-moisture atmospheric river region and the broader cloudy-sky region, with improvements mainly concentrated in the middle and lower troposphere.

What are the implications of the main findings?

- The results demonstrate the potential of using reliable clear-sky profiles to guide the enhancement of cloudy-sky humidity-profile products.
- The proposed framework provides a case-based proof of concept for humidity-profile enhancement during atmospheric river events and broader cloudy-sky conditions, while additional independent cases and observations are needed to establish its general applicability.

Abstract

Atmospheric rivers (ARs) are characterized by high water vapor content and are frequently accompanied by extensive cloud cover, creating a need for reliable humidity profiles under cloudy conditions. Fengyun-4B/Geostationary Interferometric Infrared Sounder (FY-4B/GIIRS) products provide relatively accurate clear-sky humidity profiles, whereas Fengyun-3E/Vertical Atmospheric Sounding System (FY-3E/VASS) products offer all-sky coverage but retain appreciable humidity errors. This study develops a clear-sky FY-4B/GIIRS-guided framework to enhance cloudy-sky FY-3E/VASS humidity profiles. Spatiotemporally collocated clear-sky profiles are first used to construct humidity residuals, from which principal component analysis extracts a low-dimensional residual basis. A neural network then predicts the corresponding coefficients to generate a baseline correction. Target-day calibration and cloud-condition adjustment further adapt this clear-sky-derived correction to cloudy-sky samples on the target day. The framework is evaluated against ERA5 reanalysis for a preidentified AR event along the eastern coast of China on 6 July 2023, using cloudy-sky samples from the 09:31–09:41 UTC FY-3E overpass. For all cloudy-sky

Check for updates

Academic Editor: Tamas Várnai

Received: 27 July 2026
Revised: 21 September 2026
Accepted: 5 October 2026
Published: 9 October 2026

Copyright: © 2026 by the authors. Licensee MDPI, Basel, Switzerland. This article is an open access article distributed under the terms and conditions of the Creative Commons Attribution (CC BY) license.

samples from this overpass, the pressure-level-averaged root mean square error (RMSE) decreases by 16.1% over 300–900 hPa and by 20.8% over 700–900 hPa. For cloudy-sky samples in the high-moisture AR subset, the corresponding reductions are 19.7% and 26.6%, respectively. The overlap between the high-moisture masks defined using integrated water vapor (IWV) from FY-3E/VASS and ERA5 increases from 60.7% to 73.9%. The enhanced profiles therefore show improved agreement with ERA5, particularly over 700–900 hPa, and better represent the high-moisture portion of the examined AR event.

Keywords: FY-3E/VASS; FY-4B/GIIRS; humidity profile; profile enhancement; atmospheric river; low-dimensional residual; cloud-condition adjustment

1. Introduction

Atmospheric rivers (ARs) are an important form of organized water vapor transport in midlatitudes and are often associated with extreme precipitation events. They are typically characterized by long, narrow corridors of strong horizontal water vapor transport and are closely associated with strong moisture convergence and persistent cloud systems [1–3]. Water vapor within AR regions also exhibits important vertical stratification, and the middle and lower troposphere below approximately 700–800 hPa contains most of the AR water vapor transport [4]. Errors in humidity profiles affect the representation of the vertical moisture structure of ARs. Therefore, reliable humidity-profile data are essential for analyzing AR water vapor transport and vertical moisture structure, as well as the spatial patterns of integrated water vapor (IWV) and integrated vapor transport (IVT).

Satellite atmospheric sounding products provide an important data source for monitoring humidity profiles over large areas [5], but different types of satellite products have distinct strengths and limitations. The Fengyun-4B (FY-4B)/Geostationary Interferometric Infrared Sounder (GIIRS) Level-2 Atmospheric Vertical Profile (L2 AVP) product is retrieved from hyperspectral infrared observations [6,7] and can provide relatively accurate humidity profiles under clear-sky conditions. However, AR events are often accompanied by extensive cloud systems, and clouds substantially reduce the quality and availability of hyperspectral infrared profile products [8]. The Fengyun-3E (FY-3E)/Vertical Atmospheric Sounding System (VASS) L2 AVP product is a multisensor retrieval that combines observations from the Hyperspectral Infrared Atmospheric Sounder-II (HIRAS-II), Micro-Wave Temperature Sounder-III (MWTS-III), and Micro-Wave Humidity Sounder-II (MWHS-II), which provides all-sky atmospheric temperature and humidity profiles and can monitor cloudy AR regions. Although hyperspectral infrared observations are also used in the FY-3E/VASS L2 AVP retrieval, this multisensor product is less accurate than the FY-4B/GIIRS L2 AVP product at selected middle- and lower-tropospheric pressure levels where AR moisture is concentrated. Therefore, based on the all-sky coverage capability of FY-3E/VASS, this study uses relatively accurate clear-sky FY-4B/GIIRS humidity profiles as guidance to enhance FY-3E/VASS humidity profiles and transfers the learned correction to cloudy AR regions on the target day.

To illustrate the advantage of clear-sky FY-4B/GIIRS humidity profiles as guidance and to determine the applicable pressure levels, the humidity profiles of spatiotemporally collocated clear-sky FY-3E/VASS and FY-4B/GIIRS samples are separately compared against ERA5. As shown in Figure 1, the root mean square error (RMSE) of FY-4B/GIIRS is clearly lower than that of FY-3E/VASS over 700–900 hPa, where AR moisture is concentrated. Below 900 hPa, however, FY-4B/GIIRS has larger errors than FY-3E/VASS, even though this layer also contains substantial AR moisture, and is therefore unsuitable as

a guiding source. Accordingly, clear-sky FY-4B/GIIRS humidity profiles are used only to guide corrections at and above 900 hPa; the enhanced profile remains identical to the original FY-3E/VASS humidity profile below 900 hPa. FY-4B/GIIRS also performs slightly worse than FY-3E/VASS over 500–600 hPa. Considering that this difference is small and this layer is not a primary layer of AR moisture concentration, FY-4B/GIIRS profiles over 500–600 hPa are still used as guidance to preserve vertical continuity with the layers. The 700–900 hPa layer is both a major layer of AR moisture concentration and the range in which FY-4B/GIIRS clearly outperforms FY-3E/VASS; it is therefore the main focus of the profile enhancement.

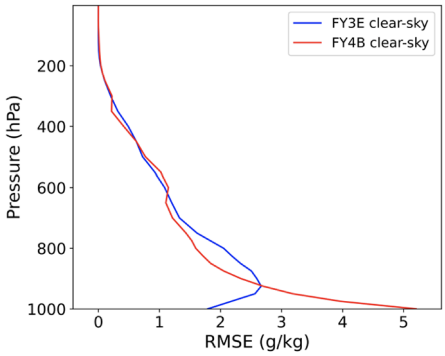

Figure 1. Root mean square error (RMSE) comparison of Fengyun-3E/Vertical Atmospheric Sounding System (FY-3E/VASS) and Fengyun-4B/Geostationary Interferometric Infrared Sounder (FY-4B/GIIRS) humidity profiles against ERA5 under clear-sky conditions.

Previous studies on humidity-profile enhancement have often focused on improving retrievals from the raw observations of a single sensor or on combining multisource raw observations in a joint retrieval [9,10]. Fewer studies have enhanced existing satellite products, especially by jointly using different product types from two different satellite platforms. Accurate humidity profiles are important for cloudy weather events such as ARs and for cloudy environments in general. Most current studies directly enhance cloudy-sky humidity profiles using raw observations acquired under cloudy conditions. Because both the measurements and retrievals are affected by complex cloud interference, the improvement is often limited [8].

This study proposes a clear-sky-guided residual-correction framework for improving FY-3E/VASS humidity-profile products under cloudy conditions. Spatiotemporally collocated FY-3E/VASS and FY-4B/GIIRS samples are first constructed. Principal component analysis is used to extract a low-dimensional basis of the humidity residuals between clear-sky FY-3E/VASS and FY-4B/GIIRS profiles. A neural network is then trained to predict the corresponding residual coefficients from FY-3E/VASS profile information and to generate a baseline correction. Target-day calibration and cloud-condition adjustment are further introduced to adapt the clear-sky-derived correction to cloudy samples on the target day, while a lower-level correction constraint keeps the profile unchanged at pressure levels greater than 900 hPa. Because water vapor is sparse above 300 hPa and the enhanced profile remains identical to the original FY-3E/VASS profile below 900 hPa, the evaluation focuses on 300–900 hPa and 700–900 hPa. The 300–900 hPa range is used to assess the overall atmospheric humidity profile, whereas 700–900 hPa represents the main layer of AR moisture concentration. ERA5 humidity profiles are used as the reference, with RMSE as the primary metric and the mean absolute error (MAE), bias, and correlation coefficient (R) as supplementary metrics. The evaluation uses FY-3E samples from the China overpass between 09:31 and 09:41 UTC on 6 July 2023, during an AR event along the eastern coast of China. Evaluations are conducted for cloudy-sky samples within the high-moisture

AR evaluation subset and for all cloudy-sky samples from the FY-3E overpass. The results demonstrate that the framework improves middle- and lower-tropospheric humidity profiles for both the cloudy high-moisture AR subset and all cloudy-sky samples from the FY-3E overpass. Although the evaluation is limited to one event and ERA5 is not an independent observational reference, the present study provides a case-based proof of concept demonstrating the potential of clear-sky-guided residual correction for cloudy-sky humidity-profile enhancement. Additional independent cases are required to establish the broader applicability of the framework.

2. Data and Case Study

2.1. Data

2.1.1. FY-3E/VASS L2 AVP Product

FY-3E is a polar-orbiting meteorological satellite in the Fengyun-3 series and is the world's first operational meteorological satellite in an early-morning orbit [11,12]. It carries several atmospheric sounding instruments (HIRAS-II, MWTS-III, and MWHS-II) and supplements observations from conventional morning- and afternoon-orbiting polar satellites, and provides important data for global numerical weather prediction, climate monitoring, and atmospheric sounding. HIRAS-II provides hyperspectral infrared atmospheric sounding information, MWTS-III provides microwave temperature sounding information, and MWHS-II provides microwave humidity sounding information. The combined use of infrared and microwave observations improves the all-sky availability of atmospheric temperature and humidity profiles.

This study uses the temperature and humidity profiles in the FY-3E/VASS L2 AVP product. The product combines observations from multiple FY-3E atmospheric sounding instruments to generate vertical temperature and humidity profiles at 37 standard pressure levels from 1 to 1000 hPa, with a spatial resolution of approximately 14~16 km. Because it provides better profile coverage in cloudy regions, the FY-3E/VASS humidity profile is the product to be enhanced in this study.

To distinguish the profiles before and after correction, the uncorrected FY-3E/VASS L2 AVP humidity-profile product is referred to as the original FY-3E/VASS humidity profile, and the corrected product is referred to as the enhanced FY-3E/VASS humidity profile.

2.1.2. FY-4B/GIIRS L2 AVP Product

FY-4B is a geostationary meteorological satellite in the Fengyun-4 series and provides continuous, high-temporal-resolution observations over China and surrounding regions [6,7]. As one of the payloads, GIIRS is directly related to atmospheric humidity sounding, measuring atmospheric radiance spectra by infrared interferometry and sounding vertical structures of atmospheric temperature and humidity [7].

This study uses the humidity profiles in the FY-4B/GIIRS L2 AVP product which contains 101 pressure levels from 0 to 1100 hPa with a spatial resolution of approximately 12 km. The product includes a cloud-mask variable that distinguishes clear-sky from cloudy samples. As an infrared sounder, the profile quality is sensitive to clouds. Therefore, only clear-sky FY-4B/GIIRS humidity profiles are used as correction guidance for the FY-3E/VASS samples [8].

The FY-3E/VASS L2 AVP product also includes cloud-classification information, but the information is more complex than the binary clear/cloudy classification required by the proposed framework. Because the framework applies the same treatment to all cloudy samples and only requires a clear/cloudy classification, incorporating FY-3E/VASS cloud-classification information would introduce unnecessary complexity into the framework. Owing to the high temporal resolution of the FY-4B geostationary satellite, FY-3E samples

over China and surrounding regions can be matched with FY-4B samples that close in both time and space [6,7]. Therefore, the clear/cloudy status of each FY-3E/VASS sample is defined as the status of its spatiotemporally collocated FY-4B/GIIRS sample.

2.1.3. ERA5 Reanalysis

ERA5 is the fifth-generation global atmospheric reanalysis produced by the European Centre for Medium-Range Weather Forecasts (ECMWF) and released by the Copernicus Climate Change Service (C3S) [13]. It combines global observations with a numerical weather prediction model through data assimilation to provide a spatiotemporally continuous and physically consistent estimate of the atmospheric state. This study uses the ERA5 hourly data located on pressure levels. The dataset has global coverage, a horizontal resolution of $0.25^{\circ} \times 0.25^{\circ}$, a temporal resolution of 1 h, and 37 standard pressure levels from 1 to 1000 hPa.

This study mainly uses ERA5 specific humidity on pressure levels, collocated in time and space with each FY-3E/VASS sample, as the reference for humidity-profile evaluation. First, ERA5 humidity profiles are used to calculate the RMSE, MAE, bias, and R of the original and enhanced FY-3E/VASS humidity profiles. Second, IWV and IVT calculated from ERA5 are used to describe the AR background on 6 July 2023 and to define the high-moisture AR evaluation subset.

2.2. Data Preprocessing

Sample selection is performed through independent quality control of the FY-3E/VASS and FY-4B/GIIRS products. If a level does not pass quality control, that level is set to an invalid value while the other levels in the profile are retained. The sample is removed only when all levels of the profile are invalid.

The humidity and temperature profiles in both the FY-3E/VASS and FY-4B/GIIRS product files include quality-control flags that indicate retrieval quality. For FY-3E/VASS, flag 1 denotes good, flags 2 and 3 denote not bad, flag 4 denotes not good, and flag 0 or values greater than 4 denote bad. Only FY-3E/VASS humidity and temperature profiles flagged as good or not bad are used. For FY-4B/GIIRS, flag 0 denotes very good, flag 1 denotes good, flag 2 denotes bad, flag 3 denotes do not use, and flag 4 denotes unusual L1 data. Only FY-4B/GIIRS humidity profiles flagged as very good or good are used.

Data containing invalid fill values or humidity or temperature values outside the valid range are also excluded. Pressure levels below the surface are removed according to the surface pressure.

2.3. Atmospheric River Case

An AR event along the eastern coast of China on 6 July 2023 is selected as the study case. FY-3E observations from the China overpass between 09:31 and 09:41 UTC, which sample the preidentified AR event and surrounding cloudy scenes, are used as the evaluation dataset for the FY-3E/VASS humidity-profile enhancement. The overpass includes samples both inside and outside the high-moisture AR evaluation subset, allowing the enhancement to be evaluated within this subset and across all cloudy samples from the overpass.

Existing standard AR identification methods commonly use thresholds of integrated vapor transport (IVT) or integrated water vapor (IWV), together with geometric constraints such as length and aspect ratio. For example, Rutz et al. identified ARs using IVT ≥ 250 kg m^{-1} s^{-1} and length ≥ 2000 km [14]. Guan and Waliser used a seasonally and spatially varying 85th-percentile IVT threshold, a lower limit of 100 kg m^{-1} s^{-1}, a length greater than 2000 km, and an aspect ratio greater than 2 for global AR detection [15]. No single standard is used for AR identification and delineation, and the identified regions vary with the selected algorithm [16].

The purpose of this study is not to develop or benchmark an AR-detection algorithm, but to evaluate the effectiveness of FY-3E/VASS humidity-profile enhancement within a preidentified AR event. AR sample selection is therefore used only to define an evaluation subset representative of the AR event, rather than to define the AR itself. Because quality control of the FY-3E/VASS and FY-4B/GIIRS products removes some samples, the retained FY-3E/VASS samples no longer form a complete and continuous gridded field. Applying standard AR-detection algorithms with geometric requirements directly to these quality-controlled samples could introduce artificial errors in the AR sample selection. Although IWV alone does not fully define an AR, a spatially contiguous high-IWV region within a preidentified AR event can provide a useful proxy for the AR. Therefore, a case-specific, reference-based sampling criterion is used: IWV is calculated from ERA5 humidity profiles collocated with the retained FY-3E/VASS samples, and the spatially contiguous samples within the upper 10% of ERA5 IWV in the FY-3E overpass region are defined as the high-moisture AR evaluation subset. This subset is used only for evaluating the effectiveness of humidity-profile enhancement in the high-moisture portion of the preidentified AR event and is not intended as a general AR-detection criterion.

Figure 2 shows the ERA5 reference moisture fields over the FY-3E overpass region between 09:31 and 09:41 UTC on 6 July 2023, including the ERA5 IVT field, the ERA5 IWV field, and the ERA5 IWV field collocated with the quality-controlled FY-3E/VASS samples.

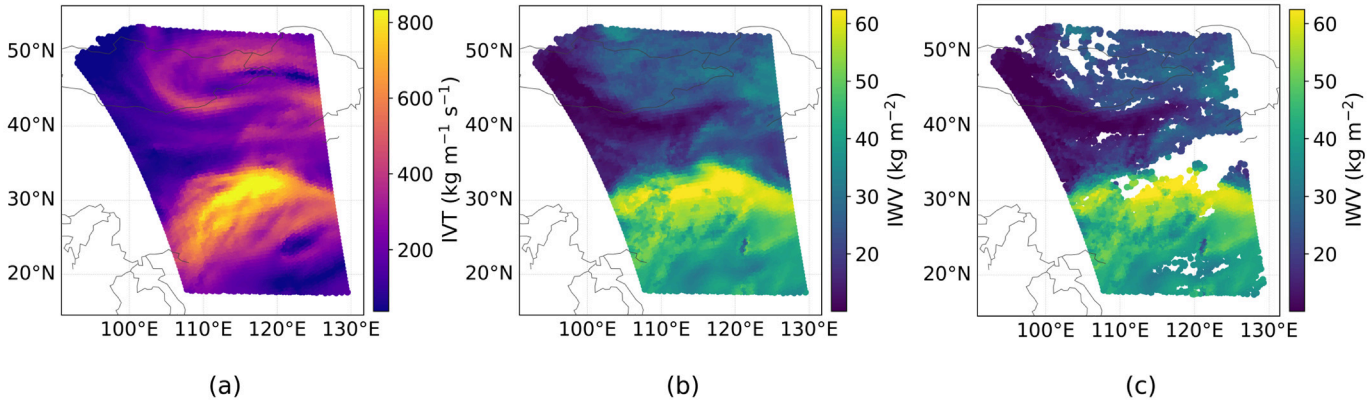

Figure 2. ERA5 reference moisture fields over the FY-3E overpass region: (**a**) Integrated vapor transport (IVT) field; (**b**) integrated water vapor (IWV) field; and (**c**) IWV field collocated with the quality-controlled FY-3E/VASS samples.

After sample screening, 13,742 valid samples of FY-3E/VASS are retained, including 2100 clear-sky samples and 11,642 cloudy-sky samples; cloudy-sky samples account for 84.7%. The ERA5-defined high-moisture AR evaluation subset contains 1374 samples, including 40 clear-sky samples and 1334 cloudy-sky samples; cloudy-sky samples account for 97.1%, confirming that the selected high-moisture AR subset is predominantly cloudy. Cloudy-sky samples in this subset are used to evaluate the effectiveness of humidity-profile enhancement within the high-moisture portion of the AR event, whereas all cloudy-sky samples from the overpass are used to provide a broader, but still case-specific, cloudy-sky evaluation.

3. Methods

3.1. Spatiotemporal Collocation and Vertical Interpolation

FY-3E/VASS is a 37-level profile product from a polar-orbiting satellite, whereas FY-4B/GIIRS is a 101-level profile product from a geostationary satellite. The two products

differ in observation time, spatial location, and pressure levels. Spatiotemporally collocated sample pairs are therefore constructed, and their pressure grids are unified.

Collocation uses each FY-3E/VASS sample as the reference and searches FY-4B/GIIRS samples for candidate matches. The thresholds are an observation-time difference Δt of no greater than 1800 s and a spatial distance d of no greater than 50 km. These thresholds are used to define a sufficiently broad candidate search window because FY-3E/VASS and FY-4B/GIIRS have different orbit configurations and observation characteristics. Stricter thresholds may reduce the number of available candidate matches. When multiple candidates are available, the best match is selected using the normalized combined spatiotemporal score S, as given in Equation (1), to minimize the spatial and temporal mismatches between the paired samples.

$$S = \left(\frac{d}{50\,\mathrm{km}}\right)^2 + \left(\frac{\Delta t}{1800\,\mathrm{s}}\right)^2 \tag{1}$$

For the collocated samples from the FY-3E overpass on 6 July 2023, the distributions of spatial and temporal differences are shown in Figure 3. The resulting collocations have a mean spatial distance of 16 km and a mean time difference of 720 s, with most of the collocations having spatial distances below 20 km and temporal differences below 900 s.

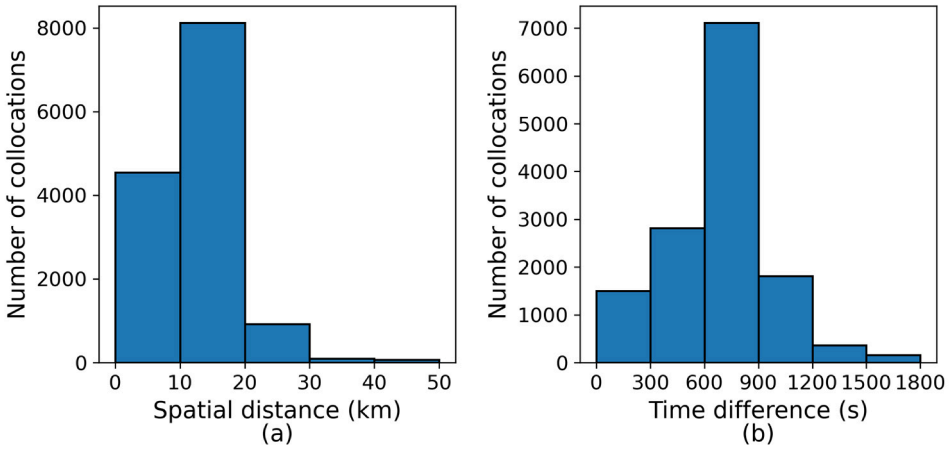

Figure 3. Distributions of FY-3E/VASS and FY-4B/GIIRS collocation differences for the samples from the FY-3E overpass on 6 July 2023: (**a**) Spatial distance; (**b**) time difference.

For vertical-grid unification, the FY-3E/VASS humidity and temperature profiles remain on their original 37-level pressure grid. As shown in Equation (2), the original 101-level FY-4B/GIIRS humidity profile is interpolated to the 37 FY-3E/VASS levels in log-pressure space. For each target FY-3E/VASS pressure level p_j, only the humidity values q_1 and q_2 at the directly adjacent upper and lower FY-4B/GIIRS pressure levels p_1 and p_2 are used to calculate the FY-4B/GIIRS humidity value $q_{FY4B}(p_j)$ at that level. If either contributing level is invalid or fails quality control, the target level is marked as invalid.

$$q_{FY4B}(p_j) = q_1 + (q_2 - q_1)\frac{\ln(p_j) - \ln(p_1)}{\ln(p_2) - \ln(p_1)} \tag{2}$$

3.2. Clear-Sky-Guided Correction Framework

This study proposes a clear-sky-guided, low-dimensional humidity-residual-correction framework. Rather than retrieving a new profile, the framework adds a low-dimensional humidity-residual-correction term to the original FY-3E/VASS humidity profile. It first constructs log-humidity residuals with a lower-level correction constraint from collocated

clear-sky FY-3E/VASS and FY-4B/GIIRS samples. Principal component analysis is then used to extract a low-dimensional residual basis. A neural network is trained to predict the corresponding low-dimensional residual coefficients from FY-3E/VASS profile information to generate the baseline correction. Target-day calibration and cloud-condition adjustment transfer the correction relationship learned from clear-sky samples to cloudy conditions on the target day, producing the enhanced FY-3E/VASS humidity profile.

3.2.1. Log-Humidity Residual and Lower-Level Correction Constraint

Let $q_{FY3E,i}(p_j)$ denote the humidity in the original FY-3E/VASS profile for collocated sample i at pressure level j, and let $q_{FY4B,i}(p_j)$ denote the humidity in the clear-sky FY-4B/GIIRS profile for sample i at pressure level j after interpolation to 37 levels. Because the magnitude of water vapor varies greatly with height, the humidity residual $r_i(p_j)$ is defined in logarithmic space to reduce these scale differences:

$$r_i(p_j) = \log\left[1 + q_{FY4B,i}(p_j)\right] - \log\left[1 + q_{FY3E,i}(p_j)\right] \tag{3}$$

FY-4B/GIIRS humidity-profile errors are relatively large below 900 hPa. Directly using near-surface FY-4B/GIIRS humidity information for guidance could therefore transfer errors from the guidance source to the enhanced FY-3E/VASS profile. A lower-level correction constraint is introduced through a vertical weighting function to limit the correction applied in the lower atmosphere. As shown in Equation (4), the vertical weight $w(p_j)$ applies the full correction when $p \leq 850$ hPa, decreases linearly over $850 < p \leq 900$ hPa, and applies no correction when $p > 900$ hPa.

$$w(p_j) = \begin{cases} 1, & p \leq 850\,\text{hPa}, \\ \frac{900-p}{900-850}, & 850\,\text{hPa} < p \leq 900\,\text{hPa}, \\ 0, & p > 900\,\text{hPa}. \end{cases} \tag{4}$$

The humidity residual with the lower-level correction constraint, $r_i^w(p_j)$, is then obtained as follows:

$$r_i^w(p_j) = w(p_j) r_i(p_j) \tag{5}$$

The lower-level correction constraint is applied throughout the framework. The final enhanced humidity profile is corrected at and above 900 hPa, while the original FY-3E/VASS humidity profile is retained below 900 hPa.

3.2.2. Low-Dimensional Humidity-Residual Basis Construction

To obtain a more stable vertical structure of the humidity-residual correction and reduce level-by-level noise, this study does not learn the humidity difference between FY-3E/VASS and FY-4B/GIIRS independently at each pressure level. Instead, a low-dimensional humidity-residual basis is constructed for the entire profile, and each residual profile derived from a collocated clear-sky sample pair is represented as a linear combination of a small number of basis profiles [17].

The target day of the AR case is 6 July 2023. Clear-sky collocated FY-3E/VASS and FY-4B/GIIRS samples from 1 to 30 June 2023 are used as the learning samples. Principal component analysis is applied to the lower-level-constrained humidity residual $r_i^w(p_j)$ of each learning sample to extract the mean residual profile $\mu(p_j)$ and K low-dimensional humidity-residual basis profiles $B_k(p_j)$:

$$r_i^w(p_j) \approx \mu(p_j) + \sum_{k=1}^{K} a_{i,k}^{\text{true}} B_k(p_j) \tag{6}$$

Because quality control may lead to missing values at individual pressure levels, a mask-aware weighted principal component analysis strategy is adopted in this study. A validity mask is first generated for each residual profile to distinguish available and unavailable pressure levels. The mean residual at each pressure level is calculated using only valid samples, while the residual profiles are weighted according to the valid-sample fraction of each pressure level. This strategy avoids artificial imputation before principal component analysis and preserves the valid vertical structures contained in the humidity-residual profiles.

The number of low-dimensional residual basis profiles is set to $K = 5$. The explained-variance ratios of the five basis profiles are 0.454, 0.222, 0.143, 0.071, and 0.045, respectively, with a cumulative explained variance of 93.5%. The five-dimensional residual coefficients retain the main vertical structure of the clear-sky humidity residuals between FY-3E/VASS and FY-4B/GIIRS while reducing the noise and vertical discontinuities that may arise from independent level-by-level correction.

3.2.3. Clear-Sky Supervised Residual-Coefficient Prediction

A one-dimensional convolutional neural network (1D CNN) is trained to predict the baseline low-dimensional humidity-residual coefficients [18]. Clear-sky collocated FY-3E/VASS and FY-4B/GIIRS samples from 1 to 30 June 2023 are again used as the training set. The neural network has three input channels: the standardized original FY-3E/VASS humidity profile, the standardized FY-3E/VASS temperature profile, and the standardized log-pressure coordinate. The humidity profile is the enhancement target, while the temperature profile and log-pressure coordinate provide additional features. The temperature profile describes the thermodynamic background, and the log-pressure coordinate explicitly represents the pressure levels and their vertical relationships.

The 1D CNN adopts a residual convolutional architecture to extract vertical features from the multi-channel atmospheric profiles. The network first applies a convolutional stem consisting of a one-dimensional convolution layer with 32 output channels, followed by group normalization and GELU activation. Five residual convolutional blocks are subsequently stacked to further extract vertical structural information. Each residual block contains two one-dimensional convolution layers with a kernel size of 5, group normalization, GELU activation, dropout with a rate of 0.05, and a residual connection. After feature extraction, the vertical features are aggregated using both mean and maximum pooling along the pressure dimension. The resulting feature vector is then mapped through a fully connected prediction head consisting of one hidden layer with 96 units and GELU activation, followed by dropout with a rate of 0.05 and an output layer that predicts five low-dimensional residual coefficients.

For each sample, the 1D CNN extracts profile features along the vertical dimension and outputs five low-dimensional residual coefficients $\hat{a}_{i,k}$. Because the data have already been preprocessed, the training loss is calculated only at valid levels of valid samples. A vertical weight is included in the loss to emphasize the middle and lower troposphere, where AR moisture is concentrated. The 300–900 hPa layer is the primary optimization range. Levels above 300 hPa contain little water vapor and are not a main AR moisture layer; assigning them excessive weight would weaken learning over 300–900 hPa, so they receive smaller weights. Levels below 900 hPa are assigned a weight of zero because of the lower-level correction constraint.

The network is trained using the AdamW optimizer with an initial learning rate of 3×10^{-4} and a weight decay of 10^{-3}. The training batch size is 1024, and the validation batch size is 2048. The maximum number of training epochs is 120, and early stopping

with a patience of 15 epochs is applied according to the validation loss. Gradient clipping with a maximum norm of 1.0 is applied to improve training stability.

After training, the model can take the original humidity profile, temperature profile, and pressure coordinate of any FY-3E/VASS sample to be enhanced and predict its low-dimensional residual coefficients $\hat{a}_k$. The previously extracted mean residual profile $\mu(p_i)$ and low-dimensional humidity-residual basis $B_k(p_i)$ are then used to reconstruct the baseline residual correction $\Delta_{\text{base},i}(p_j)$:

$$\Delta_{\text{base},i}(p_j) = \mu(p_j) + \sum_{k=1}^{K} \hat{a}_{i,k} B_k(p_j) \tag{7}$$

The baseline residual correction is subsequently combined with the target-day calibration term and the cloud-condition adjustment term to generate the final correction.

3.2.4. Target-Day Calibration

Target-day calibration reduces systematic differences between the learning samples and the target samples. Satellite product errors and atmospheric moisture conditions can vary with date and weather background, so a correction relationship learned only from historical samples may not fully represent the AR case. Cloudy-sky samples are assumed to share similar large-scale moisture-condition changes with nearby clear-sky samples when they are close in space and time. The target-day clear-sky collocated samples that are close to the cloudy-sky target samples in space and time are therefore used to calibrate the baseline residual correction. Among all overpass samples on 6 July 2023, cloudy-sky samples are the profiles to be enhanced and evaluated, whereas clear-sky samples are used to form the target-day calibration subset for estimating the calibration coefficients.

For each sample in the target-day calibration subset, the lower-level-constrained residual $r_i^w(p_j)$ is calculated from FY-3E/VASS and FY-4B/GIIRS as described above and projected onto the low-dimensional humidity-residual basis to obtain the true residual coefficients $a_{i,k}^{\text{true}}$. The trained neural network is then used to predict the low-dimensional residual coefficients $\hat{a}_{i,k}$ for the same sample. Their difference represents the systematic offset between the predicted and true residual coefficients on the target day and defines the target-day calibration coefficient $c_{\text{target},k}$:

$$c_{\text{target},k} = \text{median}\left(a_{i,k}^{\text{true}} - \hat{a}_{i,k}\right) \tag{8}$$

Here, median denotes the median of the coefficient differences over all samples in the target-day calibration subset and is used as the final target-day calibration coefficient. The median is used instead of the mean to reduce the influence of individual samples with extreme humidity or anomalous values.

The target-day calibration coefficient $c_{\text{target},k}$ and the low-dimensional humidity-residual basis $B_k(p_i)$ are used to obtain the target-day calibration term $\Delta_{\text{target},i}(p_j)$:

$$\Delta_{\text{target},i}(p_j) = \sum_{k=1}^{K} c_{\text{target},k} B_k(p_j) \tag{9}$$

3.2.5. Cloud-Condition Adjustment

In principle, the systematic structure of humidity profiles differs between cloudy-sky and clear-sky conditions, so a neural network trained on clear-sky samples cannot be directly used to predict residuals for cloudy-sky samples. In addition, the quality and availability of FY-4B/GIIRS humidity profiles are limited under cloudy conditions, making cloudy-sky samples unsuitable for supervised neural-network training. A cloud-condition

adjustment is therefore introduced to transfer the correction relationship learned from clear-sky samples to cloudy-sky samples.

All-sky FY-3E/VASS samples from 1 to 30 June 2023 are used to estimate the systematic structural difference between FY-3E/VASS humidity profiles under clear-sky and cloudy-sky conditions. This difference is then mapped to a cloud-condition adjustment coefficient in residual-coefficient space.

First, the low-dimensional structure coefficients $s_{\mathrm{cloud},i}$ and $s_{\mathrm{clear},i}$ are extracted from the humidity profiles of each cloudy-sky and clear-sky FY-3E/VASS sample, respectively. For each historical date, the difference between the median cloudy-sky profile and the median clear-sky profile is then calculated to obtain the clear–cloudy structural difference for that day. The median of these daily differences over all historical dates gives the stable historical clear–cloudy structural difference $\Delta u_{\mathrm{cloud}}$:

$$\Delta u_{\mathrm{cloud}} = \mathrm{median}[\mathrm{median}(s_{\mathrm{cloud},i}) - \mathrm{median}(s_{\mathrm{clear},i})] \tag{10}$$

To convert the clear–cloudy structural difference into an adjustment in residual-coefficient space, the historical FY-3E/VASS samples are used to fit a linear mapping from the structure coefficients $s_{\mathrm{cloud},i}$ and $s_{\mathrm{clear},i}$ to the true residual coefficients $a_{i,k}^{\mathrm{true}}$, denoted by $M_{s\to a}$. The structural difference $\Delta u_{\mathrm{cloud}}$ is then mapped into residual-coefficient space to obtain the cloud-condition adjustment coefficient $c_{\mathrm{cloud},k}$:

$$c_{\mathrm{cloud},k} = \Delta u_{\mathrm{cloud}}\, M_{s\to a} \tag{11}$$

The cloud-condition adjustment coefficient $c_{\mathrm{cloud},k}$ and the low-dimensional humidity-residual basis $B_k(p_i)$ are used to obtain the cloud-condition adjustment term $\Delta_{\mathrm{cloud},i}(p_j)$:

$$\Delta_{\mathrm{cloud},i}(p_j) = \sum_{k=1}^{K} c_{\mathrm{cloud},k} B_k(p_j) \tag{12}$$

3.2.6. Enhanced Profile Generation

Starting from the baseline residual correction $\Delta_{\mathrm{base},i}(p_j)$, the target-day calibration term $\Delta_{\mathrm{target},i}(p_j)$ and cloud-condition adjustment term $\Delta_{\mathrm{cloud},i}(p_j)$ are added to form the final residual $\Delta_{\mathrm{final},i}(p_j)$:

$$\Delta_{\mathrm{final},i}(p_j) = \Delta_{\mathrm{base},i}(p_j) + \Delta_{\mathrm{target},i}(p_j) + \Delta_{\mathrm{cloud},i}(p_j) \tag{13}$$

The final residual $\Delta_{\mathrm{final},i}(p_j)$ is added to the logarithm of the original FY-3E/VASS humidity profile, and the inverse logarithmic transformation is then applied to obtain the enhanced FY-3E/VASS humidity profile $q_{enhanced,i}(p_j)$:

$$q_{enhanced,i}(p_j) = \exp\{\log[1 + q_{FY3E,i}(p_j)] + \Delta_{\mathrm{final},i}(p_j)\} - 1 \tag{14}$$

3.3. Evaluation Design and Metrics

The evaluation data consist of cloudy samples from the FY-3E overpass over China between 09:31 and 09:41 UTC on 6 July 2023 and are used to assess the enhanced FY-3E/VASS humidity profiles under cloudy conditions at two sample-set scales: cloudy-sky samples in the high-moisture AR evaluation subset and all cloudy-sky samples from the FY-3E overpass. Specifically, IWV is calculated from ERA5 humidity profiles collocated with the FY-3E/VASS samples, and the spatially contiguous samples in the upper 10% of ERA5 IWV are selected as the high-moisture AR evaluation subset. Cloudy-sky samples within this subset are then used to evaluate profile enhancement in the high-moisture

portion of the preidentified AR event. All cloudy-sky samples from the FY-3E overpass are then evaluated to examine whether the improvement appears in the broader target-day cloudy-sky sample set.

All evaluations use ERA5 humidity profiles collocated with the FY-3E/VASS samples as the reference and include both vertical-profile evaluation and spatial AR-application evaluation. For the vertical evaluation, water vapor is sparse above 300 hPa, and the original FY-3E/VASS profile is retained below 900 hPa because of the lower-level correction constraint. Therefore, the vertical metrics focus on 300–900 hPa and 700–900 hPa. The 300–900 hPa range represents the overall atmospheric humidity profile, whereas 700–900 hPa represents the main layer of AR moisture concentration. At each pressure level, the metrics are first calculated from all valid samples and then averaged over the pressure levels within the target range. Four metrics are used: RMSE, MAE, bias, and R. RMSE and MAE describe the overall error, bias describes the systematic deviation, and R describes the linear agreement between the profiles and the reference. For the spatial AR-application evaluation, IWV is calculated separately from the original FY-3E/VASS, enhanced FY-3E/VASS, and ERA5 humidity profiles, and the resulting IWV intensity and spatial distributions are compared. The spatial overlap of the high-IWV masks derived from the original and enhanced FY-3E/VASS profiles against the ERA5-defined high-IWV AR evaluation mask is used to determine whether the enhanced profiles better represent the high-moisture portion of the preidentified AR event.

4. Results

4.1. Evaluation over the Cloudy High-Moisture AR Subset

4.1.1. Vertical-Profile Evaluation over the Cloudy High-Moisture AR Subset

To evaluate the enhanced humidity profiles in the high-moisture portion of the AR event, cloudy samples within the ERA5-defined high-moisture AR evaluation subset are used as the cloudy AR evaluation subset. Using ERA5 humidity profiles as the reference, the original and enhanced FY-3E/VASS humidity profiles are compared at each pressure level, with emphasis on 300–900 hPa and 700–900 hPa. The 300–900 hPa range represents overall atmospheric humidity, whereas 700–900 hPa represents the main layer of AR moisture concentration.

Figure 4 shows the vertical metric profiles for the cloudy high-moisture AR subset. Over 300–900 hPa, the pressure-level-averaged RMSE decreases from 2.340 to 1.879 g kg^{-1}, a reduction of 19.7%; MAE decreases from 1.976 to 1.557 g kg^{-1}; bias changes from −1.783 to −1.308 g kg^{-1}; and R increases from 0.292 to 0.452. Over 700–900 hPa, RMSE decreases from 3.573 to 2.623 g kg^{-1}, a reduction of 26.6%; MAE decreases from 3.045 to 2.162 g kg^{-1}; bias changes from −2.777 to −1.858 g kg^{-1}; and R increases from −0.077 to 0.247.

The RMSE reduction over 700–900 hPa is substantially larger than that over 300–900 hPa, indicating that the enhancement is concentrated in the middle- and lower-tropospheric moisture structure. This pressure range is both the layer in which the original FY-3E/VASS humidity profiles have a clear disadvantage relative to FY-4B/GIIRS and an important layer for moisture accumulation and transport in ARs. The results show that the proposed framework improves FY-3E/VASS humidity profiles during the cloudy AR event.

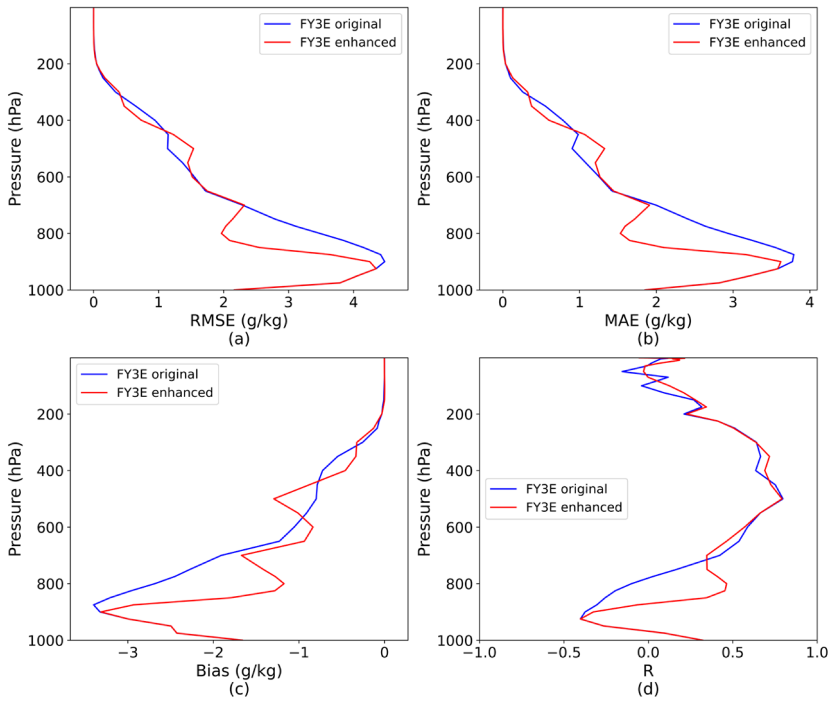

Figure 4. Vertical evaluation metrics of original and enhanced FY-3E/VASS humidity profiles against ERA5 over the cloudy high-moisture AR subset: (**a**) RMSE; (**b**) mean absolute error (MAE); (**c**) bias; and (**d**) correlation coefficient (R).

The enhanced profiles perform worse than the original profiles over 400–600 hPa, most likely because the clear-sky FY-4B/GIIRS humidity profiles are themselves less accurate than the original FY-3E/VASS profiles in this range, and this disadvantage may be propagated through the framework. However, the degradation is small relative to the overall improvement, and 400–600 hPa is not a primary AR moisture layer. The corrections over these levels are therefore retained to preserve the vertical continuity of the enhanced profiles.

4.1.2. Spatial Evaluation of High-Moisture Regions Within the AR Event

IWV is an important moisture metric for characterizing ARs. To assess whether the enhancement improves the spatial representation of the high-moisture portion of the preidentified AR event, IWV is calculated separately from the original FY-3E/VASS, enhanced FY-3E/VASS, and ERA5 humidity profiles. For each dataset, the spatially contiguous samples within the upper 10% of IWV in the FY-3E overpass region are used to form a high-moisture mask. The spatial overlap of the high-moisture masks derived from the original and enhanced FY-3E/VASS profiles with the ERA5-defined high-moisture AR evaluation mask is then compared. These masks are used only for case-specific evaluation and are not intended to define AR boundaries.

Figure 5 shows the IWV fields and high-moisture masks derived from the original FY-3E/VASS, enhanced FY-3E/VASS, and ERA5 humidity profiles. The high-moisture mask derived from the original FY-3E/VASS profiles overlaps the ERA5-defined high-moisture AR evaluation mask at 906 samples, corresponding to an overlap rate of 60.7%. For the enhanced FY-3E/VASS profiles, the overlap increases to 1102 samples and 73.9%. The enhancement therefore increases the overlap rate by 13.1 percentage points, or approximately 21.6% in relative terms. Figure 5 also shows that the high-moisture mask derived from the enhanced FY-3E/VASS profiles more closely matches the ERA5-defined high-moisture AR evaluation mask in both spatial location and shape.

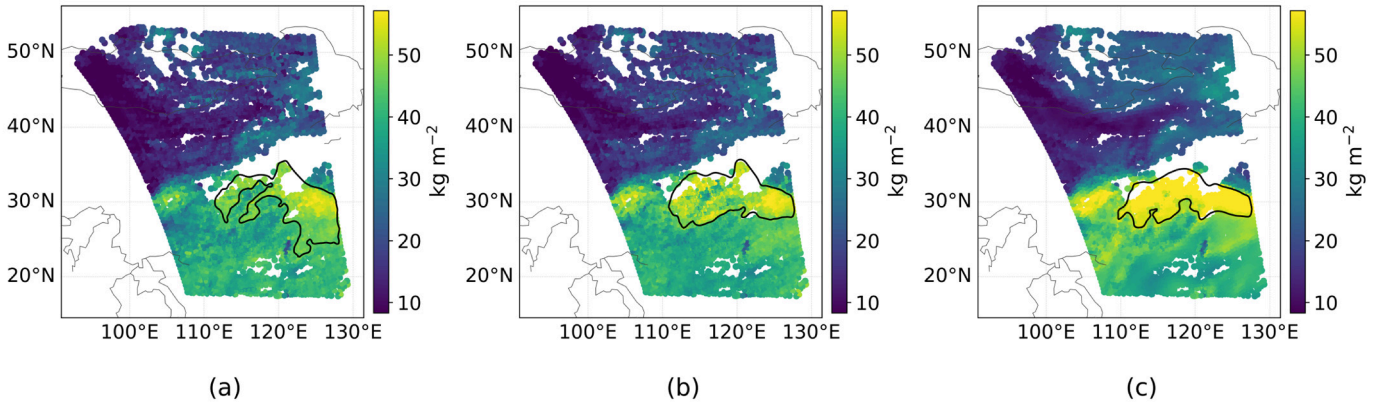

Figure 5. IWV spatial distributions and high-moisture masks within the preidentified atmospheric river event derived from different humidity profiles: (**a**) Original FY-3E/VASS; (**b**) enhanced FY-3E/VASS; and (**c**) ERA5.

These results show that the improvement is reflected not only in reduced errors at individual pressure levels but also in the horizontal distribution of high-moisture regions. After enhancement, the high-moisture mask derived from the FY-3E/VASS product is more consistent with the ERA5-defined high-moisture AR evaluation mask.

For all cloudy-sky samples in the overpass region, the 300–900 hPa partial column water vapor (PCWV) calculated from the enhanced FY-3E/VASS profiles increases from 23.58 to 24.79 kg m^{-2}, closer to the ERA5 value of 27.23 kg m^{-2}. The 700–900 hPa PCWV increases from 12.91 to 14.09 kg m^{-2}, closer to the ERA5 value of 14.74 kg m^{-2}. For cloudy-sky samples within the ERA5-defined high-moisture AR evaluation subset, the 300–900 hPa PCWV from the enhanced FY-3E/VASS profiles increases from 35.29 to 38.89 kg m^{-2}, closer to the ERA5 value of 44.70 kg m^{-2}. The 700–900 hPa PCWV increases from 18.64 to 21.25 kg m^{-2}, closer to the ERA5 value of 23.97 kg m^{-2}. Figure 6 shows the 700–900 hPa PCWV fields calculated from the original FY-3E/VASS, enhanced FY-3E/VASS, and ERA5 humidity profiles.

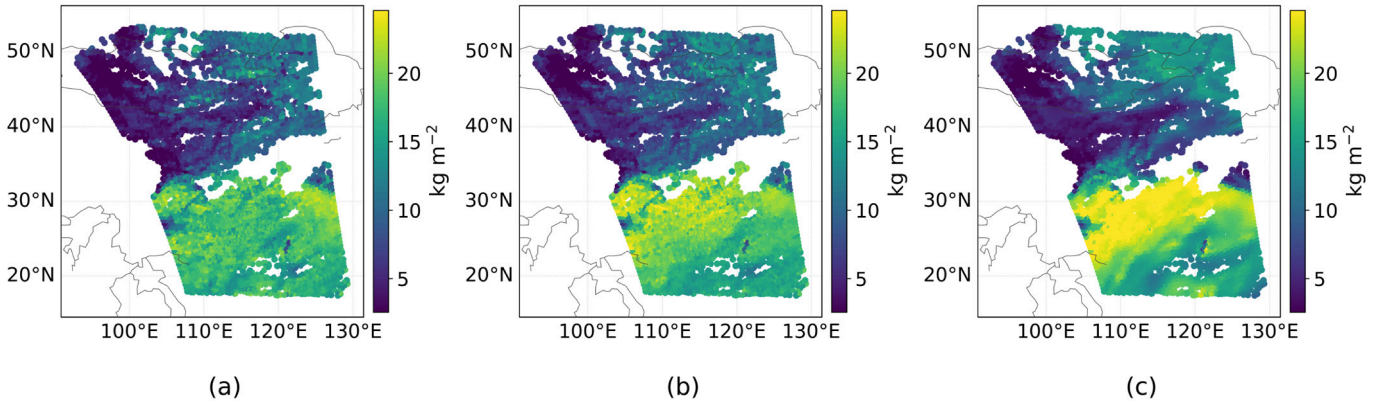

Figure 6. Spatial distributions of 700–900 hPa partial column water vapor (PCWV) derived from different humidity profiles: (**a**) Original FY-3E/VASS; (**b**) enhanced FY-3E/VASS; and (**c**) ERA5.

The PCWV results show that the enhancement over 700–900 hPa is pronounced for both all cloudy-sky samples from the overpass and the cloudy-sky samples in the high-moisture AR subset, consistent with the vertical-profile results. This indicates that the improved spatial overlap of the high-moisture masks is mainly related to improvements in middle- and lower-tropospheric water vapor content and vertical structure.

4.2. Evaluation over All Cloudy-Sky Samples

To examine the performance of the framework under more general cloudy-sky conditions, all cloudy-sky samples from the FY-3E overpass are used as the evaluation set. This set is not restricted to the high-moisture AR evaluation subset and provides a broader, but still case-specific, evaluation of cloudy-sky profile enhancement.

Figure 7 shows the vertical metric profiles for all cloudy-sky samples. Over 300–900 hPa, RMSE decreases from 1.855 to 1.557 g kg^{-1}, a reduction of 16.1%; MAE decreases from 1.484 to 1.237 g kg^{-1}; bias changes from −0.852 to −0.519 g kg^{-1}; and R increases from 0.719 to 0.784. Over 700–900 hPa, RMSE decreases from 2.845 to 2.252 g kg^{-1}, a reduction of 20.8%; MAE decreases from 2.304 to 1.804 g kg^{-1}; bias changes from −1.280 to −0.590 g kg^{-1}; and R increases from 0.651 to 0.758.

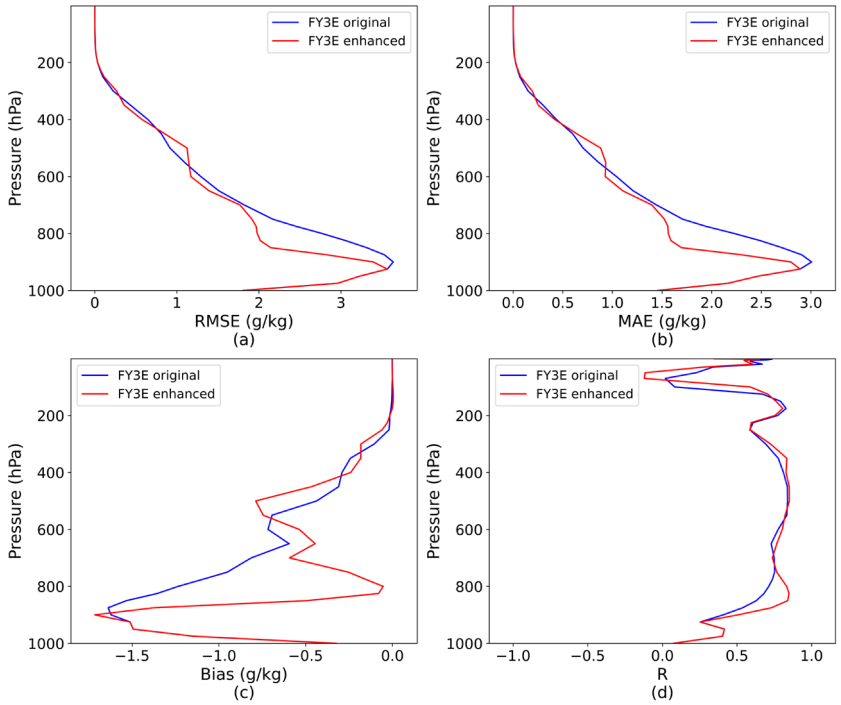

Figure 7. Vertical evaluation metrics of original and enhanced FY-3E/VASS humidity profiles against ERA5 for all cloudy-sky samples from the FY-3E overpass: (**a**) RMSE; (**b**) MAE; (**c**) bias; and (**d**) R.

As in the cloudy AR evaluation, the RMSE improvement over 700–900 hPa is clearly larger than that over 300–900 hPa for all cloudy-sky samples, indicating that the enhancement is concentrated in the middle- and lower-tropospheric moisture structure. Similarly, the enhanced profiles perform worse than the original profiles over 400–600 hPa, and the corrections over these levels are retained.

The evaluation of all cloudy-sky samples indicates that the framework improves FY-3E/VASS humidity profiles not only within the high-moisture AR subset but also across all cloudy-sky samples in this case. The improvement is most evident over 700–900 hPa, suggesting potential value for middle- and lower-tropospheric humidity monitoring in general cloudy scenes, although additional cases are needed to establish its general applicability.

5. Discussion

The results show that, when evaluated against ERA5, the proposed clear-sky-guided humidity-profile enhancement framework improves FY-3E/VASS humidity profiles in both the cloudy high-moisture AR subset and all cloudy-sky samples in this case. Compared with the original FY-3E/VASS profiles, the enhanced profiles show lower RMSE and MAE,

smaller negative bias, and higher R over both 300–900 hPa and 700–900 hPa. The improvement is particularly pronounced over 700–900 hPa, where AR moisture is concentrated.

5.1. Transfer of Clear-Sky Guidance to Cloudy-Sky Conditions

The method is based on the complementarity of the FY-4B/GIIRS and FY-3E/VASS products. FY-4B/GIIRS provides relatively accurate middle- and lower-tropospheric humidity profiles under clear-sky conditions, but its quality and availability are limited under cloudy-sky conditions. FY-3E/VASS provides better coverage in cloudy regions, but its humidity profiles can still be improved in the middle and lower troposphere, where AR moisture is concentrated. The proposed method therefore learns the low-dimensional humidity-residual structure between collocated clear-sky FY-3E/VASS and FY-4B/GIIRS samples and transfers this structure to cloudy-sky FY-3E/VASS samples to enhance their humidity profiles.

Target-day calibration and cloud-condition adjustment are the two key steps in this transfer. Target-day calibration uses target-day collocated clear-sky samples to estimate the offset in residual coefficients, thereby reducing systematic differences between the historical learning samples and the target-day samples. Cloud-condition adjustment uses the structural difference between clear-sky and cloudy-sky profiles in historical all-sky FY-3E/VASS samples to transfer the residual-correction information learned under clear-sky conditions to cloudy-sky samples.

5.2. Vertical Dependence and Lower-Level Correction Constraint

The enhancement exhibits clear vertical dependence. The improvement over 700–900 hPa is substantially larger than that over 300–900 hPa, indicating that the correction mainly affects the middle- and lower-tropospheric moisture structure. This layer is also important for AR water vapor transport and accumulation, so its improvement benefits the analysis of moisture structure in the cloudy high-moisture AR subset examined here.

The degree of improvement at different pressure levels depends not only on the framework design but also on the vertical accuracy of the guidance source. Over 700–900 hPa, clear-sky FY-4B/GIIRS humidity profiles are more accurate than FY-3E/VASS profiles, and the framework provides more stable enhancement. Over 400–600 hPa, however, clear-sky FY-4B/GIIRS profiles are slightly less accurate than FY-3E/VASS profiles, and this disadvantage may be propagated through the framework. Because the degradation over 400–600 hPa is relatively small compared with the main improvement over 700–900 hPa, and because this layer is not the primary layer of AR moisture concentration considered in this study, the corrections are retained to maintain the vertical continuity of the enhanced profiles. These results indicate that the effective vertical performance of the current implementation is closely related to the accuracy of the clear-sky guidance source.

The lower-level correction constraint is necessary to maintain the usability of the enhanced profiles. Because FY-4B/GIIRS errors are markedly larger below 900 hPa, humidity information from these levels is not used for supervision, and the original FY-3E/VASS humidity profile is retained below 900 hPa. This prevents near-surface FY-4B/GIIRS errors from being propagated into the enhanced FY-3E/VASS humidity profiles. However, the layer below 900 hPa also contributes substantially to AR moisture transport. Therefore, the absence of correction in this layer limits the ability of the current framework to provide a complete characterization of the AR moisture profile. The AR-related improvement demonstrated in the present study should consequently be interpreted primarily as an enhancement of the moisture structure within the corrected pressure range, particularly over 700–900 hPa, rather than as a complete enhancement of the full AR moisture column or near-surface moisture transport. More accurate clear-sky guidance with improved near-

surface performance may provide an opportunity to extend the effective vertical correction range in future applications.

5.3. Atmospheric River Application and Potential for Broader Cloudy-Sky Conditions

ARs are the motivation and primary application of this study, but the evaluation also includes cloudy-sky samples outside the high-moisture AR evaluation subset. The results show that the proposed framework improves middle- and lower-tropospheric humidity profiles not only within the cloudy high-moisture AR subset but also for all cloudy-sky samples from the FY-3E overpass. This suggests the potential value of the framework under broader cloudy-sky conditions.

5.4. Limitations

This study has several limitations. First, ERA5, rather than independent in situ observations, is used as the reference. Routine radiosonde observation times do not closely coincide with the FY-3E overpass examined in this study. The FY-3E overpass analyzed in this study occurred between 09:31 and 09:41 UTC, whereas routine radiosonde observations in China are generally available at 00 and 12 UTC. Therefore, the FY-3E satellite observations are temporally separated from the nearest 12 UTC radiosonde observations by approximately 2.3–2.5 h. Such a temporal mismatch may introduce additional representativeness uncertainty under the rapidly varying moisture conditions of an AR event. ERA5 was therefore used as a spatially and temporally continuous reference for the present evaluation. The reported improvement should consequently be interpreted as increased agreement between the enhanced FY-3E/VASS humidity profiles and the ERA5 reference profiles, rather than as a verified reduction in error relative to independent observational truth. Second, the effectiveness of FY-4B/GIIRS humidity profiles as guidance depends on pressure level. Limited guidance quality below 900 hPa and over 400–600 hPa constrains the enhancement range and performance. The slight degradation over 400–600 hPa indicates that errors in the guidance source may be propagated through the clear-sky-guided correction. In addition, although the layer below 900 hPa is also important for AR moisture concentration, it is not enhanced in the present framework because FY-4B/GIIRS does not provide sufficiently reliable guidance in this layer. This limits the applicability of the current implementation to complete AR moisture-profile characterization, particularly for applications requiring accurate near-surface moisture transport. Third, the evaluation of both the high-moisture AR subset and all cloudy-sky samples is based on a single FY-3E overpass on 6 July 2023. This case demonstrates the potential value of the enhanced FY-3E/VASS humidity profiles under cloudy, high-moisture conditions and in the broader cloudy-sky scene, but it cannot fully represent performance across different seasons, regions, surface types, AR intensities, or cloud regimes.

More AR cases need to be studied in the future. When more satisfactory data become available, better guidance sources should also be used for correction, and independent observations such as radiosonde profiles are recommended for evaluation.

6. Conclusions

This study proposes a humidity-profile enhancement framework guided by clear-sky FY-4B/GIIRS L2 AVP profiles to improve FY-3E/VASS L2 AVP humidity profiles under cloudy AR conditions. The framework treats the original FY-3E/VASS humidity profiles as the enhancement targets and the clear-sky FY-4B/GIIRS humidity profiles as the guidance source. It combines low-dimensional humidity-residual modeling, target-day calibration, cloud-condition adjustment, and the lower-level correction constraint to generate the enhanced FY-3E/VASS humidity profiles. The main conclusions are as follows:

1. For the preidentified AR event along the eastern coast of China on 6 July 2023, the enhanced FY-3E/VASS humidity profiles improve the middle- and lower-tropospheric moisture structure of cloudy-sky samples within the high-moisture AR evaluation subset. When evaluated against ERA5, the RMSE decreases by 19.7% over 300–900 hPa and by 26.6% over 700–900 hPa compared with the original profiles. In addition, the spatial overlap rate between the FY-3E/VASS-derived high-moisture mask and the ERA5-defined high-moisture AR evaluation mask increases from 60.7% to 73.9% after enhancement. Thus, the enhanced humidity profiles show improved pressure-level agreement with ERA5 and closer spatial agreement with the ERA5-defined high-moisture portion of the AR event.
2. For all cloudy samples from the FY-3E overpass on 6 July 2023, the enhanced profiles also show improved agreement with ERA5. The RMSE decreases by 16.1% over 300–900 hPa and by 20.8% over 700–900 hPa. These results indicate that, within the examined case, the improvement is not confined to the ERA5-defined high-moisture AR subset but also extends to broader cloudy-sky sample set. The present results should be regarded as a proof of concept for the proposed framework, and additional cases are required to establish its general applicability across different regions, seasons, and meteorological conditions.

Author Contributions: Conceptualization, J.H.; methodology, H.Y.; software, H.Y.; validation, H.Y.; formal analysis, H.Y.; investigation, H.Y.; resources, J.H.; data curation, Y.G.; writing—original draft preparation, H.Y.; writing—review and editing, J.H.; visualization, H.Y.; supervision, J.H.; project administration, J.H.; funding acquisition, J.H. All authors have read and agreed to the published version of the manuscript.

Funding: This work was funded by the National Natural Science Foundation of China (Grant No. 42575158), and funded by the Pandeng Program of the National Space Science Center, Chinese Academy of Sciences (Grant No. E5PD30041S).

Data Availability Statement: The FY-3E and FY-4B data can be downloaded from the website of the National Satellite Meteorological Center (http://satellite.nsmc.org.cn/portalsite/default.aspx, accessed on 1 April 2026). The ERA5 reanalysis dataset can be downloaded from the website of the ECMWF Climate Data Store (https://cds.climate.copernicus.eu/datasets, accessed on 1 April 2026). The processed datasets and derived data generated in this study are not publicly available because they are intermediate analysis products generated specifically for this case study.

Conflicts of Interest: The authors declare no conflicts of interest.

References

1. Ralph, F.M.; Dettinger, M.D.; Cairns, M.M.; Galarneau, T.J.; Eylander, J. Defining "Atmospheric River": How the Glossary of Meteorology Helped Resolve a Debate. *Bull. Am. Meteorol. Soc.* **2018**, *99*, 837–839. [CrossRef]
2. Gimeno, L.; Nieto, R.; Vázquez, M.; Lavers, D.A. Atmospheric Rivers: A Mini-Review. *Front. Earth Sci.* **2014**, *2*, 2. [CrossRef]
3. Payne, A.E.; Demory, M.-E.; Leung, L.R.; Ramos, A.M.; Shields, C.A.; Rutz, J.J.; Siler, N.; Villarini, G.; Hall, A.; Ralph, F.M. Responses and Impacts of Atmospheric Rivers to Climate Change. *Nat. Rev. Earth Environ.* **2020**, *1*, 143–157. [CrossRef]
4. Ralph, F.M.; Neiman, P.J.; Rotunno, R. Dropsonde Observations in Low-Level Jets over the Northeastern Pacific Ocean from CALJET-1998 and PACJET-2001: Mean Vertical-Profile and Atmospheric-River Characteristics. *Mon. Weather Rev.* **2005**, *133*, 889–910. [CrossRef]
5. Menzel, W.P.; Schmit, T.J.; Zhang, P.; Li, J. Satellite-Based Atmospheric Infrared Sounder Development and Applications. *Bull. Am. Meteorol. Soc.* **2018**, *99*, 583–603. [CrossRef]
6. Yang, J.; Zhang, Z.; Wei, C.; Lu, F.; Guo, Q. Introducing the New Generation of Chinese Geostationary Weather Satellites, Fengyun-4. *Bull. Am. Meteorol. Soc.* **2017**, *98*, 1637–1658. [CrossRef]
7. Li, J.; Menzel, W.P.; Schmit, T.J.; Schmetz, J. Applications of Geostationary Hyperspectral Infrared Sounder Observations: Progress, Challenges, and Future Perspectives. *Bull. Am. Meteorol. Soc.* **2022**, *103*, E2733–E2755. [CrossRef]

8. Li, J.; Geer, A.J.; Okamoto, K.; Otkin, J.A.; Liu, Z.; Han, W.; Wang, P. Satellite All-Sky Infrared Radiance Assimilation: Recent Progress and Future Perspectives. *Adv. Atmos. Sci.* **2022**, *39*, 9–21. [CrossRef]
9. Huang, P.; Guo, Q.; Han, C.; Tu, H.; Zhang, C.; Yang, T.; Huang, S. An Improved Method Combining CNN and 1D-Var for the Retrieval of Atmospheric Humidity Profiles from FY-4A/GIIRS Hyperspectral Data. *Remote Sens.* **2021**, *13*, 4737. [CrossRef]
10. Hu, J.; Wu, J.; Petropoulos, G.P.; Bao, Y.; Liu, J.; Lu, Q.; Wang, F.; Zhang, H.; Liu, H. Temperature and Relative Humidity Profile Retrieval from Fengyun-3D/VASS in the Arctic Region Using Neural Networks. *Remote Sens.* **2023**, *15*, 1648. [CrossRef]
11. Zhang, P.; Hu, X.; Lu, Q.; Zhu, A.; Lin, M.; Sun, L.; Chen, L.; Xu, N. FY-3E: The First Operational Meteorological Satellite Mission in an Early Morning Orbit. *Adv. Atmos. Sci.* **2022**, *39*, 1–8. [CrossRef]
12. Zhang, P.; Hu, X.; Sun, L.; Xu, N.; Chen, L.; Zhu, A.; Lin, M.; Lu, Q.; Yang, Z.; Yang, J.; et al. The On-Orbit Performance of FY-3E in an Early Morning Orbit. *Bull. Am. Meteorol. Soc.* **2024**, *105*, E144–E175. [CrossRef]
13. Hersbach, H.; Bell, B.; Berrisford, P.; Hirahara, S.; Horányi, A.; Muñoz-Sabater, J.; Nicolas, J.; Peubey, C.; Radu, R.; Schepers, D.; et al. The ERA5 Global Reanalysis. *Q. J. R. Meteorol. Soc.* **2020**, *146*, 1999–2049. [CrossRef]
14. Rutz, J.J.; Steenburgh, W.J.; Ralph, F.M. Climatological Characteristics of Atmospheric Rivers and Their Inland Penetration over the Western United States. *Mon. Weather Rev.* **2014**, *142*, 905–921. [CrossRef]
15. Guan, B.; Waliser, D.E. Detection of Atmospheric Rivers: Evaluation and Application of an Algorithm for Global Studies. *J. Geophys. Res. Atmos.* **2015**, *120*, 12514–12535. [CrossRef]
16. Shields, C.A.; Rutz, J.J.; Leung, L.-Y.; Ralph, F.M.; Wehner, M.; Kawzenuk, B.; Lora, J.M.; McClenny, E.; Osborne, T.; Payne, A.E.; et al. Atmospheric River Tracking Method Intercomparison Project (ARTMIP): Project Goals and Experimental Design. *Geosci. Model Dev.* **2018**, *11*, 2455–2474. [CrossRef]
17. Jolliffe, I.T.; Cadima, J. Principal Component Analysis: A Review and Recent Developments. *Philos. Trans. R. Soc. A* **2016**, *374*, 20150202. [CrossRef] [PubMed]
18. Kiranyaz, S.; Avci, O.; Abdeljaber, O.; Ince, T.; Gabbouj, M.; Inman, D.J. 1D Convolutional Neural Networks and Applications: A Survey. *Mech. Syst. Signal Process.* **2021**, *151*, 107398. [CrossRef]

Disclaimer/Publisher's Note: The statements, opinions and data contained in all publications are solely those of the individual author(s) and contributor(s) and not of MDPI and/or the editor(s). MDPI and/or the editor(s) disclaim responsibility for any injury to people or property resulting from any ideas, methods, instructions or products referred to in the content.